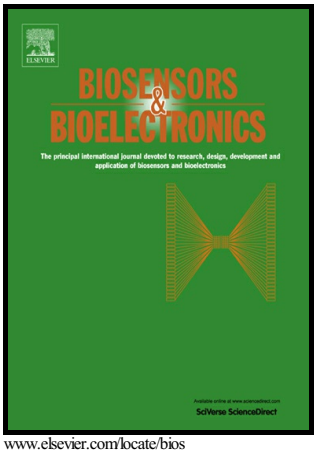

www.elsevier.com/locate/bios

Direct electrochemistry of cytochrome c immobilized on titanium nitride/multi-walled carbon nanotube composite for amperometric nitrite biosensor

Yuvaraj Haldorai, Seung-Kyu Hwang, Anantha-Iyengar Gopalan, Yun Suk Huh, Young-Kyu Han, Walter Voit

PII: S0956-5663(15)30705-3
DOI: http://dx.doi.org/10.1016/j.bios.2015.12.054
Reference: BIOS8284

To appear in: *Biosensors and Bioelectronic*

Received date: 28 September 2015
Revised date: 17 November 2015
Accepted date: 16 December 2015

Cite this article as: Yuvaraj Haldorai, Seung-Kyu Hwang, Anantha-Iyengar Gopalan, Yun Suk Huh, Young-Kyu Han and Walter Voit, Direct electrochemistry of cytochrome c immobilized on titanium nitride/multi-walled carbon nanotube composite for amperometric nitrite biosensor, *Biosensors and Bioelectronic,* http://dx.doi.org/10.1016/j.bios.2015.12.054

Direct electrochemistry of cytochrome c immobilized on titanium nitride/multi-walled carbon nanotube composite for amperometric nitrite biosensor

Yuvaraj Haldorai,[a,b*] Seung-Kyu Hwang,[c] Anantha-Iyengar Gopalan,[d] Yun Suk Huh,[c*] Young-Kyu Han,[b*] Walter Voit,[a,e*]

[a]*Department of Materials Science and Engineering, University of Texas at Dallas, Richardson TX 75080, USA*

[b]*Department of Energy and Materials Engineering, Dongguk University-Seoul, Seoul 100-715, Republic of Korea*

[c]*Department of Biological Engineering, Biohybrid Systems Research Center (BSRC), Inha University, Incheon, 402-751, Republic of Korea*

[d]*Research Energy Institute of Advanced Technology, Kyungpook National University, Daegu 702-701, South Korea*

[e]*Alan G MacDiarmid Nanotech Institute, University of Texas at Dallas, Richardson TX, USA*

Fax: +1-972-883-5725; Email: walter.voit@utdallas.edu (W. V.)

Fax: +82-2-2268-8550; Email: ykenergy@dongguk.edu (Y.-K. H)

Fax: +82-32-872-4046; Email: yunsuk.huh@inha.ac.kr (Y. S. H.)

Abstract

In this report, titanium nitride (TiN) nanoparticles decorated multi-walled carbon nanotube (MWCNTs) nanocomposite is fabricated via a two-step process. These two steps involve the decoration of titanium dioxide nanoparticles onto the MWCNTs surface and a subsequent thermal nitridation. Transmission electron microscopy shows that TiN nanoparticles with a mean diameter of ≤ 20 nm are homogeneously dispersed onto the MWCNTs surface. Direct electrochemistry and electrocatalysis of cytochrome c immobilized on the MWCNTs-TiN composite modified on a glassy carbon electrode for nitrite sensing are investigated. Under optimum conditions, the current response is linear to its concentration from 1 µM to 2000 µM with a sensitivity of 121.5 µA μM^{-1} cm^{-2} and a low detection limit of 0.0014 µM. The proposed electrode shows good reproducibility and long-term stability. The applicability of the as-prepared biosensor is validated by the successful detection of nitrite in tap and sea water samples.

Keywords: Carbon nanotubes, Titanium nitride, Nanocomposite, Cytochrome c, Nitrite sensor

1. Introduction

Carbon nanotubes (CNTs) have been of great interest since their discovery by Iijima in 1991 (Iijima and Ichihashi, 2006). CNTs containing unique structural, mechanical, thermal, and electronic properties have attracted considerable research interest, particularly for their use in nanocomposite materials for electronic and industrial applications (Iijima and Ichihashi, 2006). In addition, the application of multi-walled carbon nanotubes (MWCNTs) has been found to enhance electrocatalytic activity because of the presence of edge-plane-like sites located at both ends and in the defect region (Periasamy et al., 2014; Miao et al., 2005). In the last decade, transition metal nitrides have attracted considerable interest owing to their excellent physical and chemical properties, which makes them useful across a wide range of applications (Hargreaves, 2013). Among the transition metal nitrides, titanium nitride (TiN) has attracted significant research interest because of its simple synthesis, chemical resistance, and superior conductivity. TiN shows excellent performance in dye-sensitized solar cells (Zhang et al., 2012), supercapacitors (Dong et al., 2011), lithium-ion batteries (Wang et al., 2012), and a multitude of biosensors (Dong et al., 2011. The unique combinatorial properties of TiN, such as its superior electrical conductivity over other materials and its outstanding oxidation and acid corrosion resistance (Qiu et al., 2005), greatly benefit the preparation of electrocatalysts for direct methanol fuel cells (Avasarala et al., 2009). Taking into account the excellent individual properties of MWCNTs and TiN, a combination of the two is expected to yield enhanced performance.

Various studies have reported on the synthesis of CNTs-TiN nanocomposites for different applications. Jiang et al. (Jiang and Gao, 2006) fabricated MWCNTs-TiN composites with enhanced electrical and electrochemical properties. They also reported that MWCNTs-TiN composites possess enhanced thermal properties (Jiang and Gao, 2008). Higgins et al.

synthesized TiN-CNTs core-shell composites as effective electrocatalyst supports for low temperature fuel cells (Higgins et al., 2012). Achour et al. (Achour et al., 2014) prepared hierarchical CNTs/TiN composite electrodes for micro-supercapacitors. While TiN has been proved as a biocompatible material for coating in biomedical applications [Dion et al., 1993; Serro et al., 2009], Although CNTs/TiN composites have been used for various applications, reports of using CNTs/TiN composites as biosensors are scarce in the literature.

Cytochrome c (Cyt c), a pseudo-spherical basic redox protein with relatively small size (2.6 nm × 3.2 nm × 3.0 nm), plays the special physiological function by transferring electrons between Cyt c reductase and Cyt c oxidase both embedded in the mitochondrial membrane (Hartmann, 2005; Oellerich et al., 2002; Ochiai, 1997). Due to its electron transfer capability, Cyt c has been used potentially in electro-analytical application as the third generation protein-based electrochemical biosensors to detect some small molecules.

Nitrite ions are notable inorganic, toxic pollutants found in food, soil, water, and physiological systems. High concentrations of nitrite ions can originate from caustic radioactive waste (Coleman et al., 1995). Excess nitrite ions are detrimental to the human body, and high concentrations in drinking water pose a serious health risk to infants in particular. In the human body, nitrites can combine with hemoglobin to form methemoglobin, a harmful material that leads to a condition commonly known as “blue baby syndrome”. Nitrite can also be converted into nitrosamine, which causes cancer and hypertension (Pandikumar et al., 2014). These hazards highlight the importance of monitoring toxic nitrite ions in the environment. Various analytical methods have been used for nitrite measurement. However, electrochemical sensors have the advantages of high sensitivity, relatively good selectivity, and rapid response (Mani et al., 2012). Recently, nitrite sensors have been constructed using immobilized proteins or enzymes in nanomaterials while taking advantages

of quantum size and surface effects (Dinesh et al., 2014). The large surface area of nanomaterials provides sufficient active sites to facilitate the immobilization of proteins or enzymes and a satisfactory microenvironment to retain their bioactivity (Zhang et al., 2004).

In this study, we successfully fabricated a MWCNTs-TiN nanocomposite via a two-step process. The bio-electrochemistry of Cyt c immobilized at the MWCNTs-TiN modified glassy carbon (GC) electrode for nitrite sensing was studied. Electrochemical experiments indicated that the electrode showed a fast current response to nitrite, a wide linear range, and a low detection limit. In addition, the composite electrode exhibited excellent reproducibility and shelf-life. The electrochemical sensor showed excellent detection of nitrite in tap water and sea water samples.

2. Experimental

2.1. Materials

MWCNTs (>90% pure with a diameter of 10-20 nm and length of 0.1–10 μm), sodium nitrite ($NaNO_2$), and titanium (IV) isobutoxide (Ti(OBu)) were purchased from Sigma-Aldrich and used as received. All other organic reagents were of analytical grade and were used as received.

2.2. Oxidation of MWCNTs

The oxidation of MWCNTs was carried out according to our previous procedure (Pham et al., 2011). First, 0.5 g of MWCNTs was dispersed in 80 ml of concentrated H_2SO_4 and HNO_3 with a volume ratio of 3:1 using an ultrasonicator for 30 min. The mixture was then heated at 70^{o}C for 5 h and washed several times with deionized water until the pH reached 7. The resultant acid-functionalized MWCNTs was filtered using a 0.2 μm PTFE membrane filter

and dried in a vacuum at 70^{o}C for 24 h. This treatment produced carboxylic groups (-COOH) on the surface of the MWCNTs.

2.3. Synthesis of MWCNTs-TiO_2 nanocomposite

The synthesis process of MWCNTs-TiO_2 nanocomposite followed the previous procedure Haldorai et al., 2015). In a typical experiment, 0.5 g of the MWCNTs was ultrasonically dispersed in 250 ml of ethanol for 3 h. The mixture was then transferred to a stir plate and 5 ml of titanium butoxide was added and allowed to mix constantly for approximately 30 min. 5 ml of deionized water was then added and allowed to mix for another 30 min. The entire mixture was then refluxed for 6 h where deposition of the titanium dioxide (TiO_2) precursor occurred on the surface of the MWCNTs. After cooling, the products were filtered, washed, and annealed under nitrogen protection at 400^{o}C for 4 h to produce the MWCNTs-TiO_2 nanocomposite.

2.4. Synthesis of MWCNTs-TiN nanocomposite

The MWCNTs-TiO_2 nanocomposite prepared above was loaded into a silica tube reactor placed in a horizontal tube furnace and connected to a gas feed system. Initially, a flow of nitrogen gas was maintained over the bed to remove all air and water. After a brief waiting period (30 min) to stabilize the gas flow, the furnace was heated from room temperature to 800°C at a rate of 20°C/min. After reaching the desired reaction temperature, the flowing gas was switched to NH_3 (100 cm^3/min) and the reaction was carried out for 4 h. Finally, the MWCNTs- TiN nanocomposite product was collected after the furnace was cooled via purging nitrogen gas. The weight ratio of MWCNTs to TiN in the composite was found to be 2:1.

2.5. Fabrication of MWCNTs-TiN/Cyt c modified electrode

The MWCNTs-TiN nanocomposite modified GC electrode was prepared as follows: first, the GC electrode surface was polished with 0.3 μm alumina slurries, rinsed thoroughly with de-ionized water, sonicated in water and acetone, and air dried. Two mg of MWCNTs-TiN nanocomposite was dispersed in 5 ml of ethanol containing 0.1% nafion using ultrasonication for 30 min. A 5 μl aliquot of this dispersion was dropped on the GC electrode surface and the solvent was evaporated at ambient temperature. Second, Cyt c was immobilized by dropping a 5 μl aliquot of a 0.5 mg ml^{-1} Cyt c solution prepared in 0.1 M PBS of pH 7 onto the modified electrode surface and letting the solvent evaporate at room temperature. The electrode was then rinsed with double-distilled water two or three times to remove any loosely-bound Cyt c and allowed to dry at ambient temperature. The enzyme-modified electrode was stored in 0.1 M PBS (pH 7) at 4°C when not in use. TEM image of Cyt c immobilized on the MWCNTs-TiN composite is shown in Fig. S1.

2.6. Electrochemical analysis

Electrochemical performance was evaluated using a three-electrode cell system. Cyclic voltammetry (CV) and chronoamperometry analyses were conducted on an IVIUMSTAT and COMPACTSTAT electrochemical workstation at room temperature. A 0.1 M PBS solution served as the electrolyte, while the MWNT-TiN nanocomposite served as the working electrode. A platinum wire was employed as a counter electrode, with an Ag/AgCl (saturated KCl) electrode as the reference.

2.7. Characterization

Micro Raman measurements were taken on a WITEC alpha 300R microscope with an excitation wavelength of 532 nm. The spectrum was recorded in the range of 100 – 2000 cm^{-1}. Transmission electron microscopy (TEM, JEOL 2100F) was performed with an accelerating voltage of 200 kV and equipped with an energy-dispersive X-ray spectrometer (EDS). The

sample for the TEM observation was prepared by the deposition of an ethanolic dispersion on a 200 mesh copper grid and left to air dry. X-ray diffraction (XRD, PANalytical) was performed using Cu Kα radiation. X-ray photoelectron spectroscopy (XPS, Perkin Elmer PHI 5600) was performed using an Al X-ray source. In the XPS data analysis, peak deconvolution was performed using Gaussian components following a Shirley background subtraction.

3. Results and Discussion

3.1. Synthesis, structural, morphological, and surface studies

The MWCNTs-TiN nanocomposite was prepared via a two-step process. In the first step, the TiO_2 precursor was deposited onto the surface of acid-functionalized MWCNTs, then annealed in nitrogen at 400^{o}C for 4 h to produce the MWCNTs-TiO_2 nanocomposite.

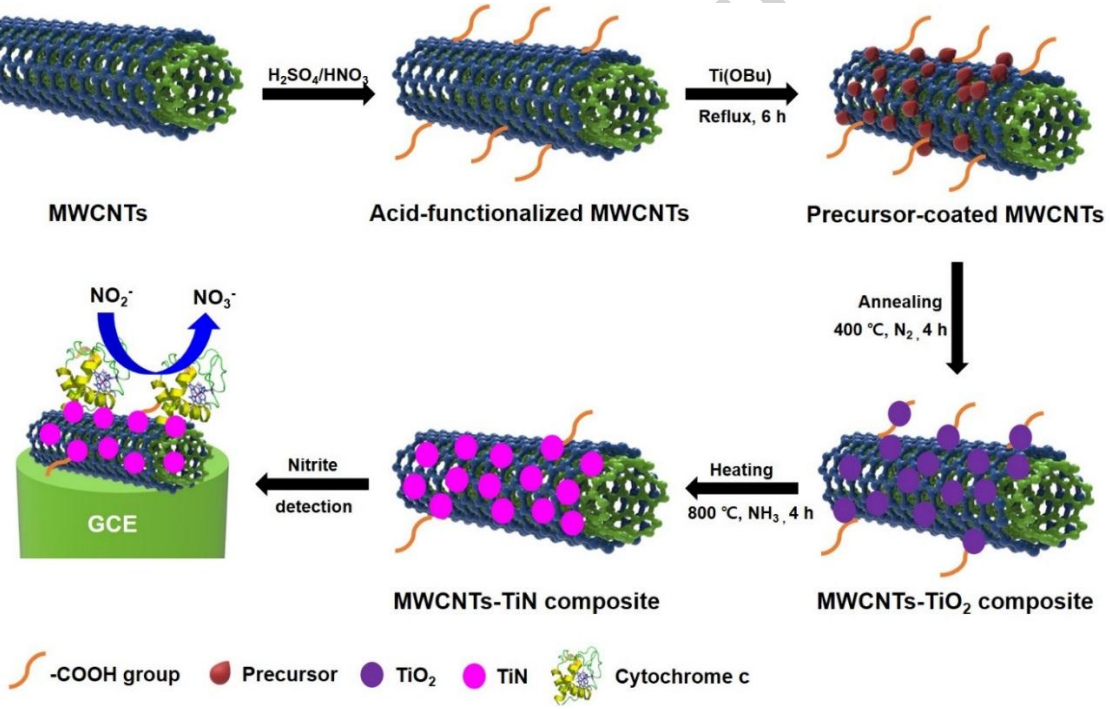

Fig. 1 (a) Schematic diagram for the synthesis of MWCNTs-TiN composite for nitrite sensing.

The acid-functionalized MWNT was able to act as a nucleating site for the growth of TiO_2 nanoparticles. In the second step, the thermal nitridation of MWCNTs-TiO_2 was carried out using ammonia at 800^{o}C for 4 h to produce the MWCNTs-TiN nanocomposite. Fig. 1 presents a schematic diagram for the fabrication of the MWCNTs-TiN nanocomposite for nitrite detection.

Fig. 2a illustrates the Raman spectrum of the MWCNTs-TiN nanocomposite. The composite exhibited two broad bands, D and G, at 1350 and 1584 cm^{-1}, respectively. The D band represents the disorder carbon arising from structural defects, while the G band corresponds to the E_{2g} phonon of sp^2 carbon atoms (Tang et al., 2009). In addition, the bands at 137, 403, 519, and 636 cm^{-1} were assigned to TiN Raman scattering. The low frequency bands at 137 and 403 cm^{-1} were caused by acoustical phonons, and the high frequency bands at 519 and 636 cm^{-1} were attributed to optical phonons (Spengler et al., 1978). Fig. 2b shows the XRD patterns of the MWCNTs-TiN nanocomposite. The composite showed diffraction peaks at 36.9, 42.8, 62.4, 74.7, and 78.8°, which were indexed to the (111), (200), (220), (311), and (222) crystal planes of TiN, respectively with a face-centered cubic structure (JCPDS No. 38-1420). No other peaks were observed, except for a strong peak at approximately 26.4° which corresponded to the (002) plane of the MWCNTs, indicating that the pure TiN nanoparticles were decorated on the MWCNTs surface. These results demonstrate the existence of both MWCNTs and TiN in the as-synthesized composite.

Fig. 2c-2f shows the TEM morphology and EDS of the MWCNTs-TiN nanocomposite. The deposition of TiN nanoparticles on the MWCNTs surface was relatively uniform and dense, as shown in Fig. 2c. In some regions, TiN nanoparticles were aggregated. Most of the TiN nanoparticles were considerably spherical in shape. However, few nanoparticles were hexagonal in shape with an average particle size of $\leq$ 20 nm (Fig. 2d). HRTEM image (Fig.

2e) shows that the interplanar distance of the TiN nanocrystal was approximately 0.254 nm, which corresponded to the (111) plane of TiN. The chemical composition of the MWCNTs-TiN nanocomposite was examined by EDS (Fig. 2f). These results confirm the presence of C, O (from MWCNTs), Ti, and N (from TiN) in the composite.

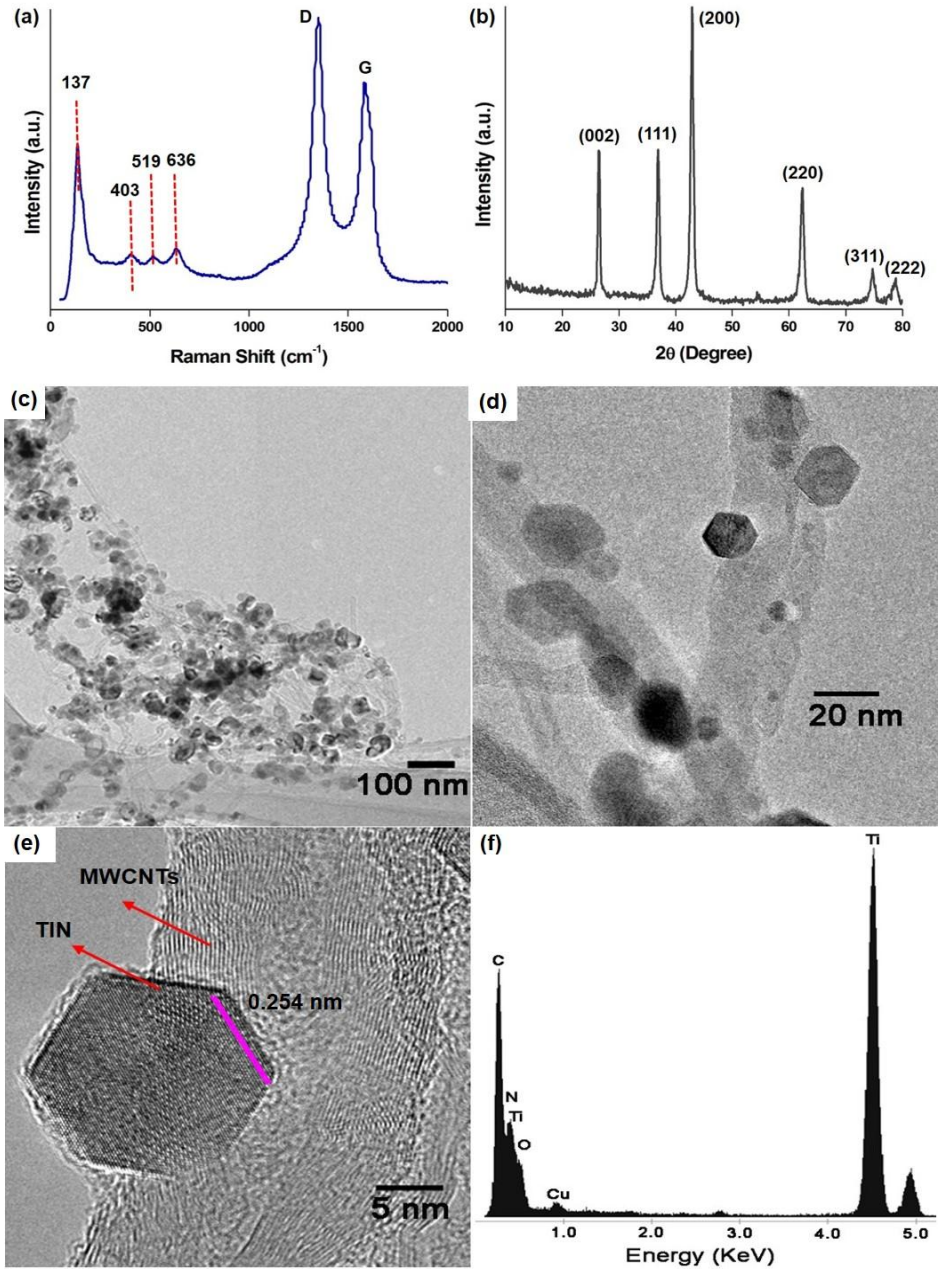

Fig. 2 (a) Raman spectrum (b) XRD pattern, (c, d) TEM, (e) HRTEM, and (f) EDS of the composite.

Fig. S2a shows the XPS survey spectrum of the as-synthesized MWCNTs-TiN nanocomposite. The spectrum exhibits four main peaks: C1s (283.6 eV), N1s (394.7), O1s (528.9 eV), and Ti 2p (457.0 eV), which confirmed the coating of TiN nanoparticles on the MWCNTs surface. The Ti 2p binding energy region had two peaks (Fig. S2b): one at a binding energy of 458.5 eV, which corresponded to the Ti $2p_{3/2}$; and another at 463.9 eV represented the Ti $2p_{1/2}$. Fig. S2c shows the C1s core level spectrum of the composite. The spectrum was analyzed using a peak fit program, and peak deconvolution was performed. The peaks were deconvoluted into Gaussian components using appropriate positions and full width at half maximum. The C1s spectrum of composite exhibited three main peaks corresponding to the carbon atom in different functional groups. The peaks at 284.2, 285.7, and 287.3 eV were ascribed to non-oxygenated C−C, C−O (hydroxyl), and C=O, respectively (Haldorai et al., 2015). As compared to the functionalized MWCNTs, the peak intensities of C−O and C=O in the C1s spectrum of the composite decreased dramatically due to thermal reduction. Further, the peak usually observed at around 290.0 eV that corresponded to the -COOH group disappeared completely. Fig. S2d shows the N1s spectrum of the composite, which was deconvoluted into four peaks. The peak with a binding energy at 396.1 eV was attributed to nitridic N from TiN, while the other three peaks corresponded to pyridine-like N (396.9 eV), pyrrole-like N (397.3 eV), and graphite-like N (398.8), respectively (Wen et al., 2011).

3.2. Electrocatalytic activity

Fig. 3a represents the CV responses of MWCNTs-GC, MWCNTs-TiN/GC, MWCNTs/Cyt c/GC, and MWCNTs-TiN/Cyt c/GC electrodes in 0.1 M KCl containing 10 mM of $Fe(CN)_6^{3-/4-}$ redox couple. The symmetrical anodic and cathodic peaks associated with the oxidation and reduction of ferricyanide-ferrocyanide reactions were observed to have much higher peak

currents at the MWCNTs-TiN/GC and MWCNTs-TiN/Cyt c/GC electrodes than the electrodes not containing TiN. This confirms that TiN augments the electroactivity of the electrode. From Fig. 3a, it was evident that the MWCNTs-TiN/Cyt c/GC electrode showed an oxidation current of 389 μA, which was close to the oxidation current of 434 μA at the MWCNTs-TiN/GC electrode. At the MWCNTs-TiN/GC and MWCNTs-TiN/Cyt c/GC electrodes, the ratios of anodic/cathodic peaks currents approached close to unity, indicating that both ferro and ferricyanide were stable in the solution and confirming the reversibility of the electrode process.

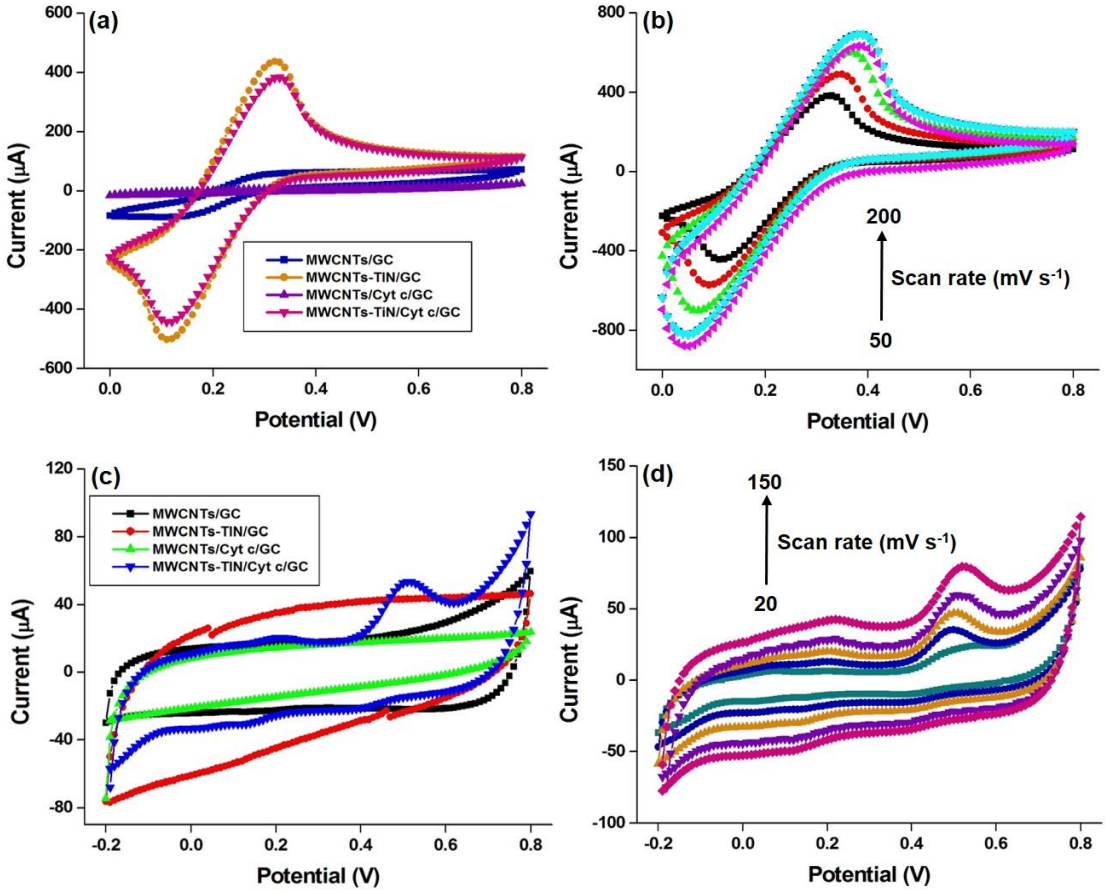

Fig. 3 (a) CVs of different electrodes in 0.1 M KCl containing 10 mM of ferro-ferri cyanide solution at a scan rate of 100 mV s^{-1}, (b) CVs of the MWCNTs-TiN/Cyt c/GC electrode in 0.1 M KCl containing 10 mM of ferro-ferri cyanide solution at various scan rates (50, 80, 120, 160, and 200 mV s^{-1}, (c) CVs of different electrodes in a 0.1 M PBS (pH 7) solution at a scan

rate of 100 mV s^{-1}, and (d) CVs of the MWCNTs-TiN/Cyt c/GC electrode in 0.1 M PBS (pH 7) at various scan rates (20, 50, 80, 100, and 150 mV s^{-1}).

These results showed an important indication that the MWCNTs-TiN/GC electrode not only exhibited good electroactivity but also provided an adequate support for the immobilized Cyt c to exhibit the electron transfer process of ferro/ferri cyanide reactions. Notably, the MWCNTs-TiN/GC electrode showed a similar oxidation current even after the immobilization of an insulating Cyt c.

To understand the kinetics of the electron transfer process at the MWCNTs-TiN/Cyt c/GC electrode (Fig. 3b), CVs of the electrode in 0.1 M KCl containing a 10 mM $Fe(CN)_6^{3-/4-}$ solution were recorded at scan rates from 50 to 200 mV s^{-1}. The separation between anodic and cathodic peaks increased with the scan rates, and the anodic/cathodic peak positions shifted gradually as the scan rate increased. These results indicate the quasi-reversible reaction of the electrode. The anodic/cathodic peak currents showed a linear increase with the scan rate, suggesting the surface-confined electron transfer process takes place at the electrode.

3.3. Electrochemical behavior of immobilized Cyt c

The electrochemical characteristics of the immobilized Cyt c molecules on the MWCNTs-TiN and MWCNTs modified GC electrodes were investigated by CV. Fig. 3c illustrates the CV behaviors of different modified electrodes in 0.1 M PBS (pH 7) at 100 mV s^{-1}. The MWCNTs-TiN/Cyt c/GC electrode exhibited a well-defined pair of quasi-reversible redox peaks. It must be noted that the MWCNTs/GC and MWCNTs-TiN/GC electrodes did not exhibit any peaks in the selected potential range between -0.20 V and 0.80 V, but very weak redox signals were observed at the MWCNTs/Cyt c electrode. These results clearly

demonstrated that the MWCNTs-TiN was successfully acted as a support matrix for the immobilization of Cyt c on the surface of the GC electrode and facilitated the electron transfer between Cyt c and the electrode. In addition, the MWCNTs-TiN support contributed effectively to the redox electron transfer of the electroactive center in the immobilized Cyt c and facilitated direct electron transfer between the Cyt c heme protein and the electrode. The formal potential of the immobilized Cyt c redox process at the MWCNTs-TiN/Cyt c/GC electrode was thus more positive than that of native Cyt c. However, it may be noted that the reversible electron exchange process of Cyt c could occur at the MWCNTs-TiN/Cyt c/GC electrode. Thus, we emphasize that the MWCNTs-TiN/Cyt c/GC exhibits direct electron transfer of Cyt c. The presence of TiN in MWCNTs-TiN makes the electrode biocompatible and provides a favorable microenvironment for the Cyt c to transfer electrons to the electrode.

Fig. 3d shows the CVs of the MWCNTs-TiN/Cyt c/GC electrode in 0.1 M PBS (pH 7) recorded at different scan rates (20 to 150 mV s^{-1}). The cathodic and anodic peak currents showed linear increase with scan rates indicated that the electrode reaction of Cyt c immobilized onto the MWCNTs-TIN composite corresponded to the surface-controlled quasi-reversible process. When the scan rate increased, the oxidation potential of Cyt c for direct electron transfer shifted to more positive potential, while the reduction peak potential shifted to more negative value. As a result, the anodic/cathodic peak separation increased with the scan rate. An estimation of the electron transfer rate constant (k_s) for the Cyt c direct electron transfer reaction was obtained from the peak potential separation values; considering the Laviron model (Laviron, 1979) for a surface-confined electron transfer process using the charge transfer coefficient (α) as 0.5 at 100 mV s^{-1} (Chen et al., 2009), the k_s value can be obtained, as shown in Eq. 1:

$$log\ k_s = \alpha \log(1-\alpha)\ + (1-\alpha) log\alpha - \log RT\ /nFv\ -\ (\alpha(1-\alpha)nF\Delta E_p)/(2.3\ RT) \quad \text{--- (1)},$$

where ΔE_p represents the peak-to-peak separation, v is the scan rate in V s^{-1}; n denotes the number of electrons transferred; R is the gas constant (8.314 J K^{-1} mol^{-1}), T is the temperature (298 K), and F is the faraday constant (96,485 C mol^{-1}). The k_s value of the MWCNTs-TiN/Cyt c/GC electrode was calculated to be 2.78 s^{-1} and was much higher than the values reported for other Cyt c modified electrodes; for example, Cyt c adsorbed on mesoporous NaY zeolite (0.78 +/- 0.04 s^{-1}) (Chen et al., 2009), mesoporous nibioum oxide (0.28 s^{-1}) (Xu et al., 2003), poly(5,2′:5,2″-terthiophene-3-carboxylic acid) (1.86 s^{-1}) (Koh et al., 2008), Au/chitosan/MWNT (0.97 s^{-1}) (Xiang et al., 2007), Au/TiO_2 (1.04 s^{-1}) (Zhoa et al., 2008), dsDNA/Au (1.4 s^{-1}) (Liu et al., 2003), and humic acid/Au (1.0 s^{-1}) (Xu et al., 2004). The higher k_s value suggests that the MWCNTs-TiN modified electrode acts as a good platform for the immobilization of Cyt c, and the modified electrode can provide a favorable microenvironment for Cyt c to undergo easy and fast electron transfer reactions even at high scan rates.

3.4. Bioelectrocatalysis for nitrite oxidation

Fig. 4a depicts the CVs obtained at the MWCNTs/GC, MWCNTs-TiN/GC, MWCNTs/Cyt c/GC, and MWCNTs-TiN/Cyt c/GC electrodes in 0.1 M PBS (pH 7) containing 20 mM of nitrite. A significant oxidation peak for the nitrite was observed at 0.92 V with a higher peak current of 195 μA for the MWCNTs-TiN/Cyt C/GC electrode, while the modified electrodes not containing Cyt c showed only a broad, weak peak around 0.90 V, attributed to nitrite oxidation. Importantly, the nitrite oxidation peak current observed for the MWCNTs-TiN/Cyt c/GC electrode was 5.1 times higher than the oxidation current (38 μA) observed for the MWCNTs/Cyt c/GC electrode. The results obtained from the comparison of electrochemical oxidation behavior of nitrite at various electrodes clearly indicated that inclusion of TiN support matrix and the immobilization of Cyt c synergistically improved the electrocatalytic

oxidation current of nitrite at the MWCNTs-TiN/Cyt c/GC electrode. We believe that the observed high current at the MWCNTs-TiN/Cyt c/GC electrode for nitrite oxidation is attributed to a combination of factors such as the accumulation of oxidative electroactive species at the thin layer of the high surface area MWCNTs, the excellent electrocatalytic property of the TiN, and the rapid electron transfer mediation from the immobilized Cyt c.

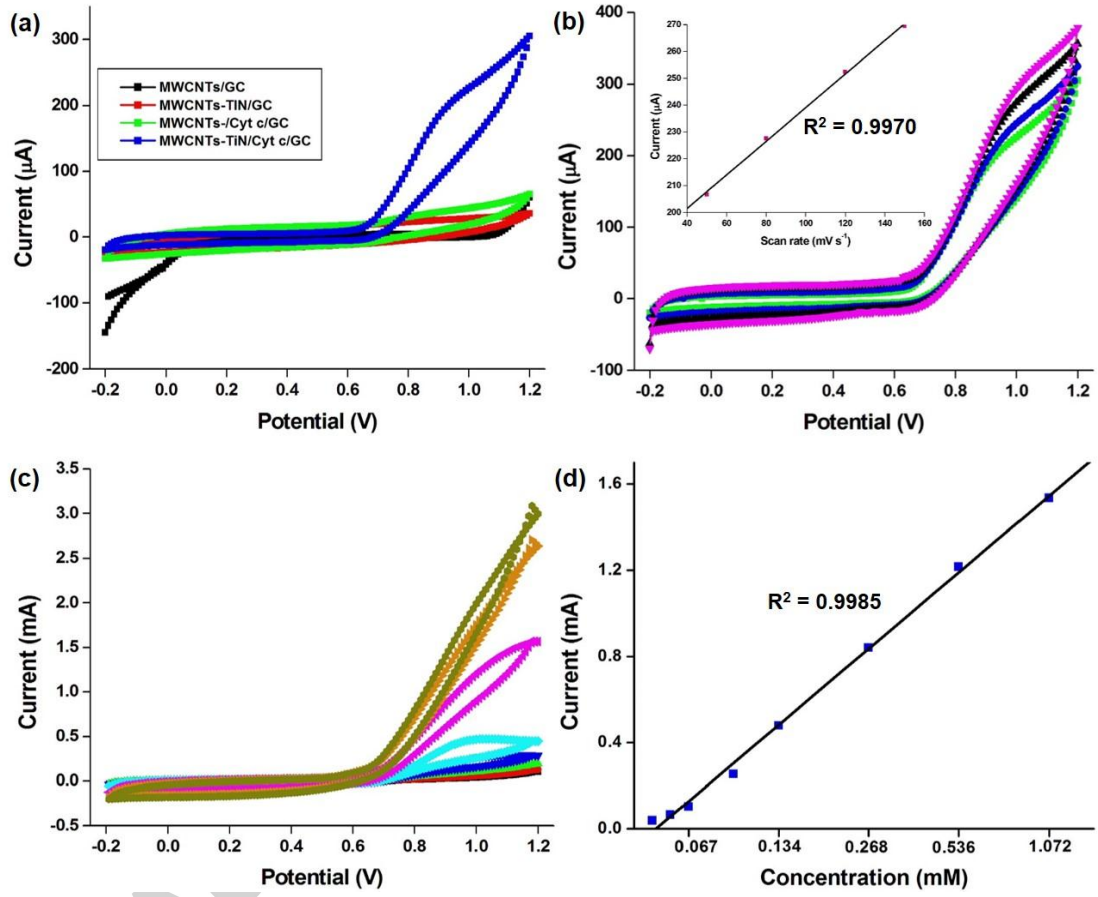

Fig. 4 (a) CVs of different electrodes in 0.1 M PBS (pH 7) in the presence of 20 mM nitrite at a scan rate of 50 mV s^{-1}, (b) CVs of MWCNTs-TiN/Cyt c/GC electrodes in PBS (pH 7) containing 20 mM nitrite at various scan rates (50, 80, 120, and 150 mV s^{-1}, inset showing the plot of anodic peak current versus scan rate), (c) CVs of MWCNTs-TiN/Cyt c/GC electrodes in 0.1 M PBS (pH 7) containing different concentrations of nitrite, and (d) the plot of anodic peak current versus concentration.

The effect of scan rate on the electrochemical oxidation of nitrite was studied to evaluate the nature of the electrochemical process taking place at the MWCNTs-TiN/Cyt c/GC electrode. Fig. 4b shows the CVs obtained for the nitrite oxidation at scan rates ranging from 50 to 150 mV s^{-1} in the presence of a 20 mM nitrite (PBS, pH 7). It was clear that the oxidation current steadily increased as the scan rate increases. The linear dependence of the nitrite oxidation peak current shown in in Fig. 4b inset indicated that the plot of the anodic peak current versus the scan rate was a straight line with a linear regression coefficient (R^2) of 0.997. This confirmed that the electrochemical oxidation of nitrite at the MWCNTs-TiN/Cyt c/GC electrode was a diffusion-controlled process. In addition, the anodic peak of the Cyt c direct electron transfer shifted to more positive value as the scan rate increased. For the irreversible and diffusion-controlled electrode process, the diffusion coefficient was calculated according to the Randles-Sevcik equation (Eq. 2), shown here:

$$i_p = kn^{3/2}AD^{1/2}Cv^{1/2} \quad \text{---------- (2),}$$

where i_p refers to the peak current in ampere, A is the electrode surface area in cm^2, n is the electro transfer number, D is the diffusion coefficient of electroactive materials, C is concentration of electroactive material in $cm^2\ s^{-1}$, and v is the scan rate in V s^{-1}. The diffusion coefficient of the MWCNTs-TiN/Cyt C/GC electrode was calculated as 2.52×10^{-5} $cm^2\ s^{-1}$. This value is in agreement with the previously reported Cyt c immobilized electrodes (Pournaghi-Azar et al., 2004).

Fig. 4c shows the CVs recorded for various concentrations of nitrite at the MWCNTs-TiN/Cyt c/GC electrode in 0.1 M PBS (pH 7). The nitrite concentration in this solution was gradually augmented by adding a calculated volume of stock nitrite solution. The anodic peak current showed a steady increase that corresponded to increasing nitrite concentrations in the

0.05 to 1.0 mM range. The anodic peak current showed a linear dependence on the concentration of nitrite (Fig. 4d) with an R^2 value of 0.9985.

The CVs recorded at the MWCNTs-TiN/GC for a 20 mM nitrite solution (PBS, pH 7) did not show pronounced peak currents (27.4 μA) for the oxidation of nitrite (Fig. 4 a). However, the oxidation peak current for nitrite at the MWCNTs-TiN/Cyt c/GC electrode (195 μA) was about ~ 7.1 times higher than that of the MWCNTs-TiN/GC electrode. This clearly indicates that the MWCNTs-TiN/Cyt c/GC electrode mediated the oxidation of nitrite predominantly. Our results therefore confirmed the bio-electrocatalytic activity of the MWCNTs-TiN/Cyt c/GC electrode. Considering the mechanistic steps proposed in the first oxidative nitrite biosensor (Geng et al., 2004) involving the predominant role of Cyt c, we hypothesize the following mechanism in three steps:

$$Fe^{2+}\text{- Cyt c} \rightarrow Fe^{3+}\text{- Cyt c} + e^{-} \text{ ---------- (3)}$$

$$Fe^{3+}\text{- Cyt c} \rightarrow [Fe^{4+}\text{- Cyt c}]^{\circledR} + 2e \text{ ---------- (4)}$$

$$[Fe^{4+}\text{- Cyt c}]^{\circledR} + NO^{2-} + H_2O \rightarrow Fe^{3+}\text{ - Cyt c} + NO^{3-} + 2H^{+} \text{---------- (5).}$$

In the first step (Eq. 3), ferrous Cyt c is oxidized to ferric form and observed at low potentials. In the second step (Eq. 4), the ferric-Cyt c is further oxidized to radical form $[Fe^{4+}\text{- Cyt c}]^{\circledR}$ at higher potentials. Eqs. 3 and 4 are the most probable as the MWCNTs-TiN/Cyt c/GC electrode exhibits a direct electron transfer process at lower potential. The highly reactive Cyt c-π cation ($[Fe^{4+}\text{- Cyt c}]^{\circledR}$) subsequently mediates the oxidation of nitrite and regenerates the reactive enzyme (Fe^{3+}- Cyt c) again (Eq. 5). Upon comparison of CV curves obtained in various concentrations of nitrite at the MWCNTs-TiN/Cyt c/GC biosensor (Fig. 4c), it was clear that the electrode was highly sensitive to nitrite concentrations. These results confirmed that the electrode can be used to bio-electrocatalytically quantify the concentration of nitrite.

3.5. Amperometric determination of nitrite

Fig. 5a represents the amperometric response of the MWCNTs-TiN/Cyt c/GC electrode to successive step–wise additions of nitrite in 0.1 M PBS. A significant increase in peak current was observed when nitrite was added to the stirred PBS. The electrode responded rapidly to the nitrite, reaching a plateau within 5 s. Fig. 5b shows the calibration curve for the nitrite. The electrode exhibited a linear relationship to the nitrite concentration (1–2000 μM), with a regression equation of I (μA) = 8.5041 C (mM) + 6.9789 (R^2 = 0.9994). The low detection limit can be calculated using the following equation (Eq. 6):

$$LOD = \frac{3S_b}{S} \text{ ---------- (6),}$$

where S_b is the standard deviation of five blank measurements and S is the sensitivity. The low detection limit and sensitivity were identified at 0.0014 μM and 121.5 μA μM^{-1} cm^{-2}, respectively. The lower detection limit could be ascribed to the positive loading of Cyt c on the MWCNTs-TiN/Cyt c/GC electrode, made possible by the present method and rapid electron transfer between Cyt c and the electrode. When the concentration of nitrite was further increased, a current plateau was observed. Together, these results indicated that the electrode had excellent nitrite detection. The comparison of linear range and detection limit of other electrodes to those of the MWCNTs-TiN/Cyt c/GC electrode is listed in Table 1. Even though previously reported enzymatic and non-enzymatic nitrite sensors based on other nanomaterials showed good performances, the superior performance of the MWCNTs-TiN/Cyt c/GC electrode may be attributed to the high surface area of the MWCNTs, the good electrocatalytic property of the TiN, and the rapid electron transfer mediation from the immobilized Cyt c.

Selectivity is an important parameter of the nitrite sensor. Various common ions, such as Mg^{2+}, $H_2PO_4^-$, Na^+, K^+, SO_4^{2-}, NO^{3-}, CO_3^{2-}, CH_3COO^-, and Cl^- did not interfere with the detection of nitrite. Fig. 5c shows that no significant amperometric responses were observed

when 2 mM each of $MgSO_4$, KH_2PO_4, $NaNO_3$, Na_2SO_4, Na_2CO_3, CH_3COONa, and KCl were injected at regular intervals. However, upon the addition of 20 μM of nitrite, a notable amperometric response was immediately produced, revealing the excellent selectivity of the MWCNTs-TiN/Cyt c/GC electrode toward nitrite determination.

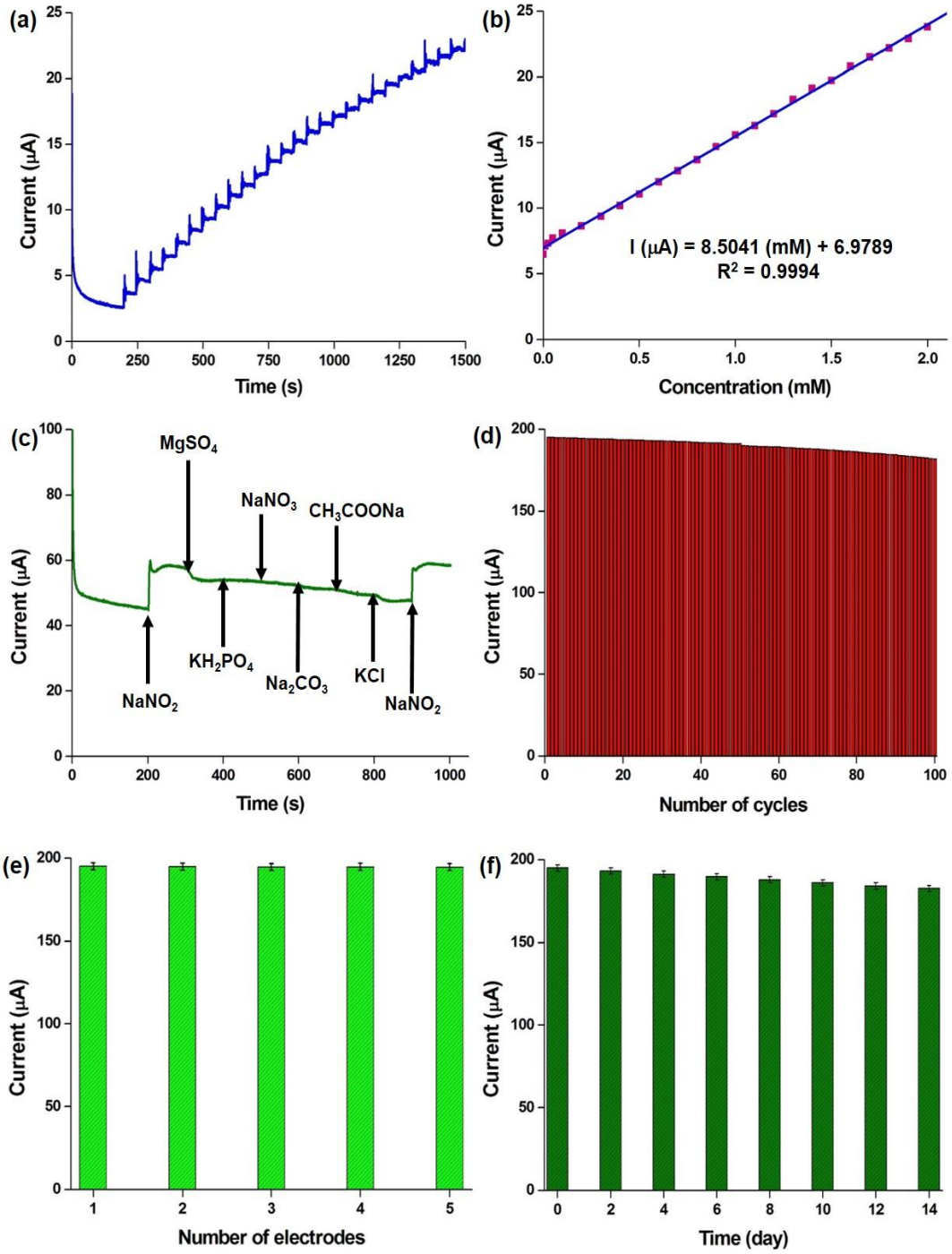

Fig. 5 (a) Chronoamperometric data of the MWCNTs-TiN/Cyt c/GC electrode with the successive addition of nitrite in 0.1 M PBS, (b) plot of peak current versus concentration, (c) interference test of the electrode with 20 μM nitrite in the presence of various common ions, (d) CV peak currents of the MWCNTs-TiN/Cyt c/GC electrode for 100 multiple cycles to detect 2 mM of nitrite at a scan rate of 50 mV s^{-1}, (e) peak currents of five different MWCNTs-TiN/Cyt c/GC electrodes to detect 2 mM of nitrite at a scan rate of 50 mV s^{-1}, and (f) shelf-life of the MWCNTs-TiN/Cyt c/GC electrode after 2 weeks.

3.6. Stability, reproducibility, and shelf-life

To demonstrate the stability of the MWCNTs-TiN/Cyt c/GC electrode, 100 cycles of CVs were carried out using 2 mM of nitrite in 0.1 M PBS. The plot of the anodic peak current versus its number of cycles (Fig. 5d) showed that the peak current falls by 7.7% even after 100 cycles, indicating the good stability of the electrode. The reproducibility of the sensor was demonstrated by the measurement of changes in the CV peak currents (Fig. 5e) of five different electrodes during nitrite (2 mM) detection. The relative standard deviation was calculated as 1.92%, indicating the good reproducibility of the electrode. The shelf-life of the MWCNTs-TiN/Cyt c/GC electrode was checked after two weeks (Fig. 5f). The electrode was stored in 0.1 M PBS (pH 7) at 4^{o}C, and the detection of nitrite (2 mM) was monitored at regular two day intervals. The high stability of the electrode may be attributed to the good chemical stability of nanocomposite in the electrolyte.

3.7. Real sample analysis

For real sample analysis, the fabricated MWCNTs-TiN/Cyt c/GC electrode sensor was used to measure nitrite levels in tap and sea water. Water samples consisting of different concentrations of spiked nitrite were quantitatively analyzed using a standard addition

method. Before analysis, the samples were filtered using a 0.2 μm filter to remove micron-sized particles. Recoveries (Table S1) were observed from 97.5% to 102.5% for 20 to 60 μM nitrite-spiked samples. These results indicated that the sensor exhibited excellent nitrite detection in tap and sea water.

Table 1. Results of the present study compared with previous reports of various electrodes for nitrite sensing.

Electrode	Detection limit (μM)	Linear range (μM)	Ref.
RGO/MWNT/Pt/Mb/GC	–	100 – 12,000	Mani et al. (2014)
Au/ZnO/MWNT/GC	0.4	0.78 – 400	Lin et al., (2011)
Cu/MWNT/CS/GC	0.024	0.1 – 2500	Yang et al., (2010)
CTAB-GO/MWNT/GC	1.5	5 – 800	Yang et al, (2014)
Cyt c/L-cysteine/Au/GC	1.5×10^{-7} (mol/L)	5×10^{-6} – 4. 5 × 10^{-4} (mol/L)	Li et al. (2008)
Mb/MWNT/cysteamine/ nafion/Au	0.1	1 – 250	Canbay et al. (2015)
Cyt c/DNA/MWNT/PAMAM/CS/GC	0.03	0.2 – 80	Chen et al. (2010)
Cyt c/ L-cysteine/P3MT/ MWNT/GC	0.5	10 – 100	Eguílaz et al. (2010)
Fe_2O_3/RGO	0.015	0.05 – 780	Radhakrishnan et al. (2014)
PEDOT/MWNT/SPCE	0.96	50 – 1000	Lin et al. (2009)
MWCNTs -TiN/Cyt c/GC	0.0014	1 – 2000	This work

RGO–reduced graphene oxide; Mb–myoglobin; CS–chitosan; CTAB–cetyltrimethylammonium bromide; PAMAM–poly(amidoamine); P3MT–poly(3-

methylthiophene); PEDOT–poly(ethylenedioxythiophene); SPCE–screen-printed carbon electrode; DPV–differential pulse voltammetry

4. Conclusions

We have successfully synthesized MWCNTs-TiN nanocomposite and investigated as an electroactive material for nitrite sensing. Cyclic voltammetry analysis showed that Cyt c immobilized on the composite and modified on a glassy carbon electrode exhibited an excellent electrocatalytic activity towards nitrite oxidation. The chronoamperometry results demonstrated that the peak current of nitrite increased linearly with concentrations from 1 to 2000 μM (R^2 = 0.9994), and had a detection limit of 0.0014 μM (S/N = 3). The fabricated sensor demonstrated excellent anti-interference abilities with good stability and reproducibility. In addition, the sensor exhibited excellent detection of nitrite in tap and sea water samples, indicating that this electrode can be effectively used for industrial sample analysis.

Acknowledgements This material was based partially upon the work supported from several sources: FUSION support from the State of Texas, CONACYT support from Mexico and the DARPA Young Faculty Award D13AP00049.

This work was also supported by the National Research Foundation of Korea (NRF) grant funded by the Korean Ministry of Science, ICT & Future Planning (2010-C1AAA001-0029018) and the Basic Science Research Program through the National Research Foundation of Korea (NRF) funded by the Ministry of Science, ICT & Future Planning (No. 2014R1A5A1009799).

Author Declaration: "Syzygy Memory Plastics, Inc. funds undergraduate research in the Advanced Polymers Research Laboratory (APRL) at the University of Texas at Dallas. Walter Voit has a significant financial interest in Syzygy Memory Plastics, Inc. This financial interest has been disclosed to UT Dallas and a conflict of interest management plan is in place to manage the potential conflicts of interest associated with this research program."

References

Achour, A., Ducros, J.B., Porto, R.L., Boujtita, M., Gautron, E., LeBrizoual, L., Djouadi M.A., Brousse, T., 2008. Nano Energy 7, 104–113.

Avasarala, B., Murray, T., Li, Haldar, W.P., 2009. J. Mater. Chem. 19, 1803-1805.

Canbay, E., Şahin, B., Kıran, M., Akyilmaz, E. 2015. Bioelectrochem. 101, 126-131.

Chen, Q., Ai, S., Zhu, X., Yin, H., Ma, Q., Qiu, Y., 2009. Biosens. Bioelectron. 24, 2991–2996.

Chen, Q., Ai, S., Fan, H., Cai, J., Ma, Q., Zhu, X., Yin H., 2010. J. Solid State Electrochem. 14, 1681-1688.

Coleman, D.H., White, R.E., Hobbs, D.T., 1995. J. Electrochem. Soc. 142, 1152–1161.

Dai, Z., Liu, S., Ju, H., 2004. Electrochim. Acta 49, 2139-2144.

Dinesh, B., Mani, V., Saraswathi, R., Chen, S., 2014. RSC Adv. 4, 28229-28237.

Dion, I., Rouais, F., Trut, L., Baquey, Ch., Monties, J.R., Havlik, P., 1993. Biomaterials 14, 169-176.

Dong, S., Chen, X., Gu, L., Zhang, L., Zhou, X., Liu, Z., Han, P., Xu, H., Yao, J., Zhang, X., Li, L., Shang, C., Cui, G., 2011. Biosens. Bioelectron. 26, 4088-4094.

Dong, S., Chen, X., Gu, L., Zhou, X., Xu, H., Wang, H., Liu, Z., Han, P., Yao, J., Wang, L., Cui, G., Chen, L., 2011. ACS Appl. Mater. Interfaces 3, 93-98.

Eguílaz, M., Agüí, L., Yánez-Sedeno, P., Pingarrón, I., 2010. J. Electroanal. Chem. 644, 30-35.

Geng, R., Zhao, G., Liu, M., Li, M., 2008. Biomaterials 29, 2794-2801.

Haldorai, Y., Rengaraj, A., Lee, J.-B., Huh, Y.S., Han, Y.-K., 2015. Synth. Met. 199, 345–352.

Hargreaves, J., 2013. Coordin. Chem. Rev. 257, 2015-2031.

Hartmann, M., 2005. Chem. Mater. 17, 4577–4593

Higgins, D.C., Choi, J.-Y., Wu, J., Lopez, A., Chen, Z., 2012. J. Mater. Chem. 22, 3727-3732.

Iijima, S., Ichihashi, T., 1993. Nature 363, 603-605.

Jiang, L., Gao, L., 2006. J. Am. Ceram. Soc. 89, 156-161.

Jiang, L., Gao, L., 2008. Ceram. Int. 34, 231-235.

Koh, W.C.A., Rahman, Md. A., Choe, E.S., Lee, D.K., Shim, Y.-B., 2008. Biosens. Bioelectron. 23, 1374–1381.

Laviron, E., 1979. J. Electroanal. Chem. Interfacial Electrochem. 100, 263-270.

Li, M.Y., Kong, L.M., Zhu, P.S., Peng, B., Huang, S.S., Yuan, Y.X., 2008. Phys. Test. Chem. Anal. B Chem. Anal. 44, 495–498.

Lin, C.-Y., Vasantha, V.S., Ho, K.-C., 2009. Sens. Actuators B, 140, 51–57

Lin, A.J., Wen, Y., Zhang, L.J., Lu, B., Li, Y., Jiao, Y.Z., Yang, H.F., 2011. Electrochim. Acta 56, 1030–1036.

Liu, H.-H., Lu, J.-L., Zhang, M., Pang, D.-W., Abruña, H.D., 2003. J. Eleelctroanal. Chem. 544, 93-100.

Mani, V., Periasamy, A P., Chen, S., 2012. Electrochem. Commun.17, 75-78.

Mani, V., Dinesh, B., Chen, S.M., Saraswathi, R., 2014. Biosens. Bioelectron. 53, 420–427.

Miao, Y., Chen, J., Hu, Y., Anal. 2005. Biochem. 339, 41-45.

Ochiai, E., 1997. J. Chem. Educ. 74, 600–604.

Oellerich, S., Wackerbarth, H., Hildebrandt, P., 2002. J. Phys. Chem. B 106, 6566–6580.

Pandikumar, A., Manonmani, S., Ramaraj, R., 2014. Catal. Sci. Technol. 2, 345–353.

Periasamy, A., Wu, W., Lin, G., Shih, Z., Yang, Z., Chang, H., 2014, J. Mater. Chem. 2, 11899-11904.

Pham, Q.L., Haldorai, Y., Nguyen, V.H., Tuma, D., Shim, J.J., 2011. Bull. Mater. Sci. 34, 37–43.

Pournaghi-Azar, M.H., Dastangoo, H., 2004. J. Eleelctroanal. Chem. 567, 211-218.

Qiu, Y., Gao, L., 2005. J. Phys. Chem. B 109, 19732-19740.

Radhakrishnan, S., Krishnamoorthy, K., Sekar, C., Wilson, J., Kim, S.J., 2014. Appl. Catal. B: Environ. 148-149, 22–28.

Serro, A.P., Completo, C., Colaço, R., dos Santos, F., Lobato da Silva, C., Cabral, J.M.S., Araújo, H., Pires, E., Saramago, B., 2009. Surf. Coat. Tech. 203, 3701-3707.

Spengler, W., Kaiser, R., Christensen, A.N., Muller-Vogt, G., 1978, Phys. Rev. B 17, 1095.

Tang, L.H., Wang, Y., Li, Y.M., Feng, H.B., Lu, J., Li, J.H., 2009. Adv. Funct. Mater. 19, 2782-2789.

Wang, Y., Ohnishi, R., Yoo, E., He, P., Kubota, J., Domen, K., Zhou, H., 2012. J. Mater. Chem. 22, 15549-15555.

Wen, Z., Cui, S., Pu, H., Mao, S., Yu, K., Feng, X., Chen, J., 2011. Adv. Mater. 23, 5445–5450.

Xiang, C., Zou, Y., Sun, L.-X., Xu, F., 2007. Talanta 74, 206-211.

Xu, X., Tian, B.Z., Kong, J.L., Zhang, S., Liu, B.H., Zhao, D.Y., 2003, Adv. Mater. 15, 1932–1936.

Xu, J.-J., Wang, G., Zhang, Q., Zhou, D.-M., Chen, H.-Y., 2004. Electrochem. Commun. 6, 278-283.

Yang, S., Liu, X., Zeng, X., Xia, B., Gu, J., Luo, S., Mai, N., Wei, W., 2010. Sens. Actuators B 145, 762–768.

Yang, Y.J., Li, W., 2014. Biosensors Bioelectron. 56, 300–306.

Zhang, M., Smith, A., Gorski, W., 2004. Anal. Chem. 76, 5045-5050.

Zhang, X., Chen, X., Dong, S., Liu, Z., Zhou, X., Yao, J., Pang, S., Xu, H., Zhang, Z., Li, L., Cui, G., 2012. J. Mater. Chem. 22, 6067-6071.

Zhao, G., Lei, Y., Zhang, Y., Li, H., Liu, M., 2008. J. Phys. Chem. C 112, 14786–14795.

Highlights

- Direct electrochemistry of cytochrome c immobilized on the MWCNTs-TiN composite
- The low detection limit for nitrite sensing was identified as 0.0014 μM
- Detection of wide range (1 to 2000 μM) of nitrite concentrations
- High stability and reproducibility of the composite electrode
- Excellent anti-interference capacity towards various common ions